

A Simple Technique for Using Radar Data in the Dynamic Initialization of a Mesoscale Model

ROBERT F. ROGERS

NOAA/AOML Hurricane Research Division, Miami, Florida

J. MICHAEL FRITSCH

Department of Meteorology, The Pennsylvania State University, University Park, Pennsylvania

WINIFRED C. LAMBERT

ENSCO, Inc., Cocoa Beach, Florida

(Manuscript received 21 April 1999, in final form 17 August 1999)

ABSTRACT

A simple technique for using radar reflectivity to improve model initialization is presented. Unlike previous techniques, the scheme described here does not infer rain rates and heating profiles from assumed relationships between remotely sensed variables and precipitation rates. Rather, the radar data are only used to tell the model when and where deep moist convection is occurring. This information is then used to activate the model's convective parameterization scheme in the grid elements where convection is observed. This approach has the advantage that the convective precipitation rates and heating profiles generated by the convective parameterization are compatible with the local (grid element) environment. The premise is that if convection is forced to develop when and where it is observed during a data assimilation period, convectively forced modifications to the environment will be in the correct locations at the model initial forecast time and the resulting forecast will be more accurate.

Three experiments illustrating how the technique is applied in the simulation of deep convection in a warm-season environment are presented: a control run in which no radar data are assimilated, and two additional runs where radar data are assimilated for 12 h in one run and 24 h in the other. The results indicate that assimilating radar data can improve a model's description of the mesoscale environment during the preforecast time period, thereby resulting in an improved forecast of precipitation and the mesoscale environment.

1. Introduction

It has long been recognized that the success of numerical simulations depends strongly on the accuracy with which the atmosphere is represented at the time of model initialization. Many researchers have proposed that this accuracy is best achieved by providing time continuity and dynamic coupling among the various fields (e.g., Charney et al. 1969), a concept that has become known as four-dimensional data assimilation (FDDA). The past few decades have seen the development of several FDDA techniques, ranging from simple, continuous direct replacement of a model variable at the nearest time step and grid point by an observation (Jastrow and Halem 1970) to more complicated meth-

ods, such as Newtonian relaxation (Lyne et al. 1982; Stauffer and Seaman 1990) and adjoint methods (Lewis and Derber 1985). When these techniques are used to generate model-balanced initial conditions, that is, dynamic initialization (Anthes 1977), the subsequent numerical prediction is often substantially improved (e.g., Stauffer and Seaman 1990).

In recent years, attention has turned toward using various sources of remotely sensed data to improve model initial conditions. For example, satellite data have been used to initialize global-scale models in the Tropics (Kasahara et al. 1994; Krishnamurti et al. 1991; Puri and Davidson 1992). In these studies, outgoing long-wave radiation (OLR) measurements were used to infer regions of precipitation and to calculate heating rates based on derived precipitation rates. Various methods were then utilized to adjust the divergence and moisture fields in order to produce the "observed" precipitation rates.

Data assimilation techniques have also been devel-

Corresponding author address: Dr. Robert F. Rogers, NOAA/AOML Hurricane Research Division, 4301 Rickenbacker Causeway, Miami, FL 33149.
E-mail: rogers@aoml.noaa.gov

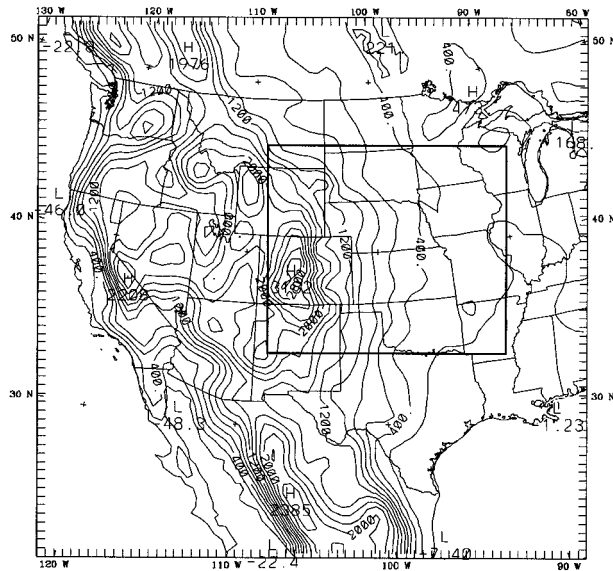


FIG. 1. Coarse mesh domain and plot of coarse mesh terrain (contour interval 250 m). Bold line indicates position of fine mesh domain.

oped for mesoscale numerical models. For example, Manobianco et al. (1994) assimilated extratropical satellite-derived data every half hour in a 9.5-h assimilation period. A relationship was derived between Special Sensor Microwave/Imager retrieved precipitation rates, which were available only twice in the assimilation period, and half-hourly infrared temperature data for calculating precipitation rates. The model-generated latent heating profile was modified (at grid locations where the data revealed precipitation) to reflect the derived precipitation rates. In locations where the data showed no precipitation, no latent heating was calculated. Two novel procedures were introduced in this research: 1) internally consistent model-generated heating profiles were scaled to produce the satellite-derived precipitation rates instead of using externally defined profiles, and 2) latent heating profiles were incorporated at grid points where the model was not producing precipitation but the satellite-derived data indicated precipitation was occurring. As a result of the data assimilation and associated forcing, forecast positions of fronts and low-level vertical motion patterns were improved.

Radar reflectivity data have also been used in data assimilation experiments with mesoscale models (e.g., Wang and Warner 1988; Takano and Segami 1993; Aonashi 1993). In Wang and Warner (1988), heating rate profiles calculated from instantaneous rain rates were determined based on the standard National Weather Service relationship for convective rainfall observations with the Weather Surveillance Radar-1957 (WSR-57), and then scaled to better match rain gauge data. These data were, as with satellite data, used to define a three-dimensional latent heating field (using externally defined profiles) that was assimilated in several dynamic initialization experiments and for a short time at the

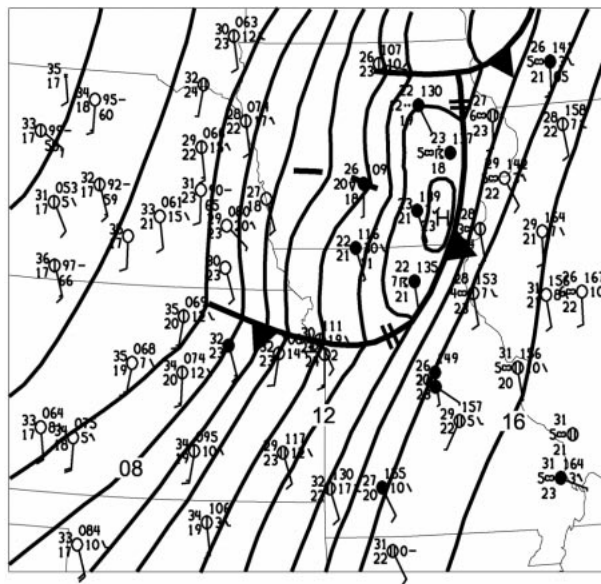
TABLE 1. Grid configurations and physical parameterizations used in the simulations. CGM denotes coarse grid mesh; FGM denotes fine grid mesh.

Domain setup	
CGM	
Grid length	54 km
(<i>x, y, σ</i>) dimensions	65 × 64 × 29
FGM	
Grid length	18 km
(<i>x, y, σ</i>) dimensions	100 × 88 × 29
Model top	100 mb
Half- σ levels	0.997, 0.991, 0.984, 0.9755, 0.9655, 0.952, 0.933, 0.908, 0.8775, 0.844, 0.808, 0.7665, 0.719, 0.6665, 0.611, 0.5555, 0.50, 0.4445, 0.389, 0.336, 0.286, 0.239, 0.1945, 0.1525, 0.1135, 0.0775, 0.0445, 0.014
Convective parameterization scheme	
CGM	Kain-Fritsch (Kain and Fritsch 1990)
FGM	Kain-Fritsch (Kain and Fritsch 1990)
PBL scheme	High-resolution Blackadar (Zhang and Anthes 1982)
Explicit moisture scheme	Water and ice physics (Zhang 1989; Dudhia 1989)

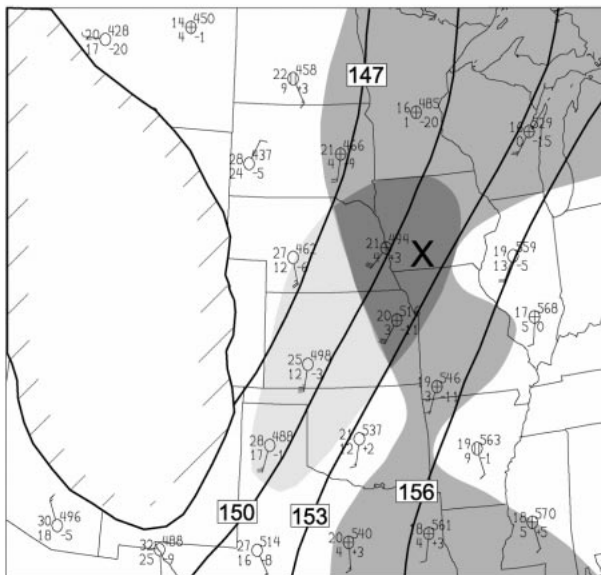
beginning of the forecast in several static initialization experiments. The quantitative precipitation forecasts from the assimilation experiments showed considerable improvement over a control forecast in which no assimilation was used.

The present study also makes use of information obtained from radar reflectivity data to help initialize a mesoscale model. However, unlike previous studies, the radar data are not used to directly infer rain rates and heating profiles. Rather, the data are only used to tell the model when and where deep moist convection is occurring. The model's convective parameterization scheme (CPS) is then manipulated to turn on or off in a manner that matches the timing and location of the observed convection. This approach has the advantage that the convective precipitation rates and heating profiles are compatible with the local (grid element) environment. The idea underlying this approach is that if convection is forced to develop when and where it is observed, its associated precipitation and circulations will be in the correct locations at the model initial forecast time and the resulting forecast will be more accurate.

In support of this approach, many studies have used three-dimensional mesoscale numerical models to demonstrate that mesoscale convective systems and their near environment evolve differently when the timing and/or location of initial convection is artificially changed (e.g., Fritsch and Chappell 1981; Zhang and Fritsch 1986; Kain and Fritsch 1992; Stensrud and Fritsch 1994b; Zhang and Harvey 1995; Rogers and Fritsch 1996). These studies clearly indicate that, in order to make accurate numerical forecasts of mesoscale weather phenomena, it is important for convective pa-



(a)



(b)

FIG. 3. (a) Surface mesoanalysis valid at 0000 UTC 16 Jul 1982. Bold dashed line indicates trough axis. (b) The 0000 UTC 16 Jul 850-mb geopotential height analysis. Light shading denotes regions with wind speeds $\geq 12.5 \text{ m s}^{-1}$. Medium shading denotes regions with dewpoint depressions $\leq 5 \text{ K}$. Dark shading over central plains denotes overlap of regions with wind speeds $\geq 12.5 \text{ m s}^{-1}$ and dewpoint depressions $\leq 5 \text{ K}$. Large X indicates the location of the MCS-generated vortex. Region over the Rocky Mountain states enclosed by the dashed line indicate areas where the surface pressure is less than 850 mb.

ifying the moisture availability of the ground where heavy rainfall had occurred prior to initialization, and modifying the relative humidity fields of the model in locations where clouds were observed (Stensrud and Fritsch 1994b; Koch et al. 1997; Rogers 1998). These changes were introduced at the beginning of the radar assimilation period for the experiments described below.

3. Description of technique

The concept of the technique, first outlined in Lambert (1994), is simple: digitized reflectivity data are used to determine the actual areas of convection in a pre-forecast period and, if necessary, force or stop the CPS in the model such that convection only occurs when and where it is observed. The two procedures used by Manobianco et al. (1994) (discussed above) will also be used here, but with a modification. Specifically, the CPS will calculate the vertical heating profile, but the heating profile will not be modified to reflect the observed precipitation rate. Instead, the heating rate will simply be that which satisfies the closure of the KF parameterization scheme.

Two situations arise when applying the technique: 1) stopping convection at locations where the data show there is no convection but the model CPS calculates there is, and 2) forcing convection to occur where the data show there is convection but the model CPS does not produce it. The first condition is treated by turning off all of the convective tendencies in the model. Treatment of the second condition involves choosing a model layer of air most likely to be the source layer for the convective cloud, forcing it to its level of free convection (LFC), and then allowing the CPS to produce the convective effects. The treatment of each of these conditions, along with procedures for the unlikely event that there is no LFC in the model sounding, are discussed in greater detail in the sections that follow.

a. Defining convective locations

The procedure begins by interpolating radar data onto the model grid. For situations where digitized radar data are available, radar coordinates must be converted to model coordinates. For situations where digitized radar is not available, the echoes must be manually digitized to the model grid. According to an analysis of the radar and lightning data from a well-documented squall line case, reflectivities above 40 dBZ were only found in the convective rain region (Meitin and Cuning 1985; Rutledge and MacGorman 1988). Therefore, this value was chosen as the threshold value indicating the presence of deep convective clouds in a given grid element. A more sophisticated indicator of the presence/absence of deep convection would likely be necessary to distinguish large reflectivity values associated with deep convection from those originating from the melting layer of heavy nonconvective precipitation.

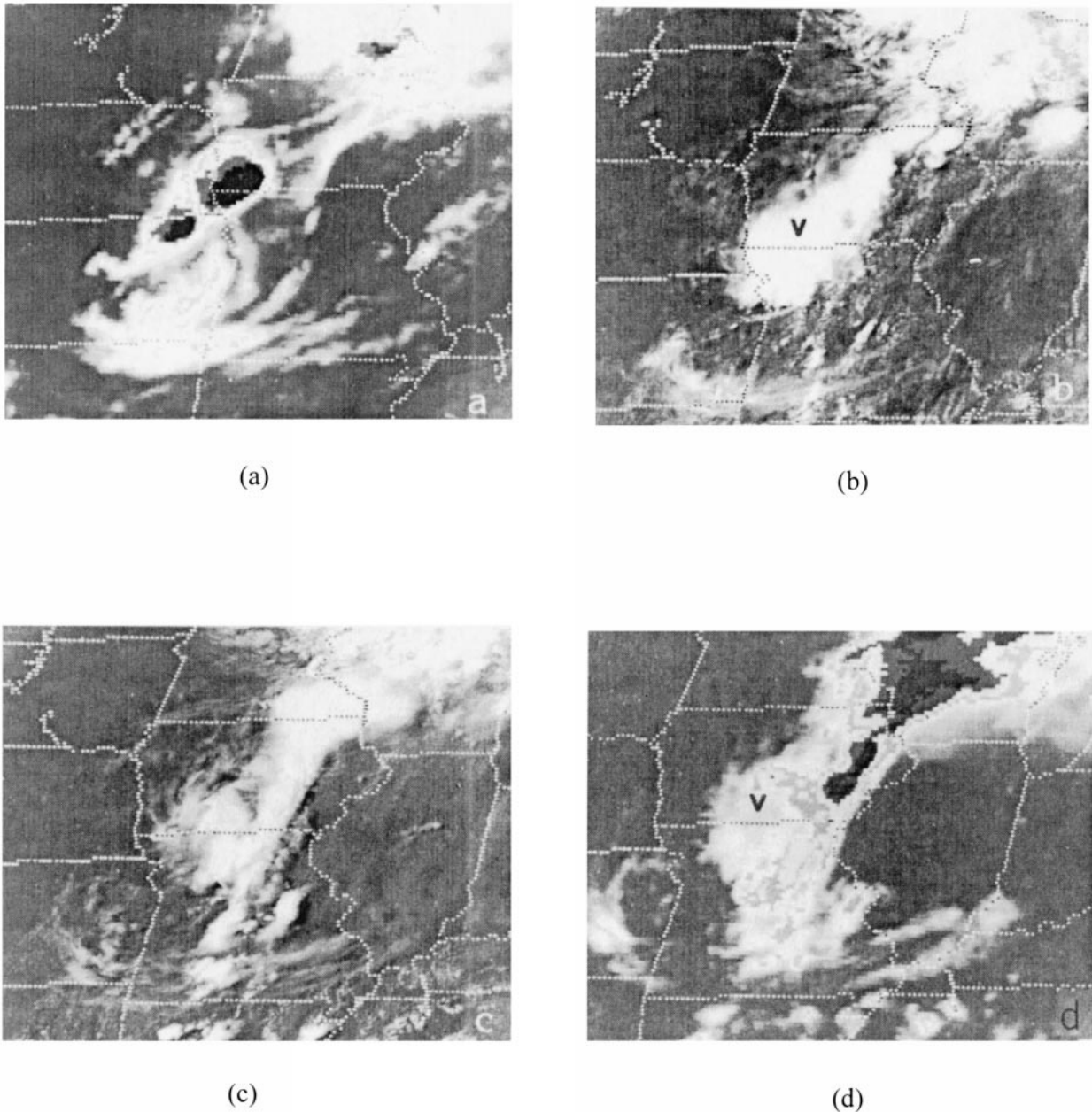


FIG. 4. Visible and enhanced infrared satellite images valid at (a) 1701 UTC, (b) 2031 UTC, (c) 2231 UTC 15 Jul, and (d) 0101 UTC 16 Jul 1982.

The radar data used in the assimilation period came from National Weather Service WSR-57 radars that were operational during the time periods in question. A 0.5° elevation scan was taken with temporal resolutions between 10 and 30 min. These scans are the observational basis for the analysis procedure. It is recognized that, to some extent, the presence of deep convection may be missed at certain grid points due to the combination of range limitations and the elevation scan angle. Nevertheless, it is believed that the radar network captured well the bulk of the convective activity.

Once the locations of deep convection are determined, a two-dimensional array indicating the presence or absence of convection in the grid boxes of the domain is created. Grid elements are flagged to indicate whether or not the radar data indicate deep convection is occurring. If no radar data are present at a grid element, the occurrence of convection is determined solely by how the CPS analyzes the model environmental conditions. This procedure is carried out for all radars that produced scans during the radar assimilation time periods.

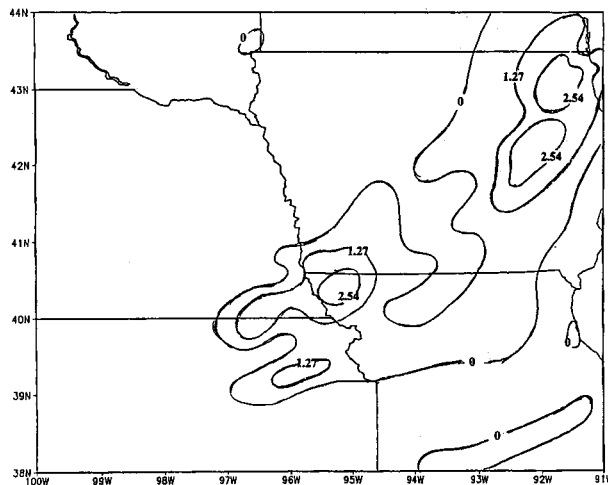


FIG. 5. Total rainfall (cm) for the 10-h period ending 0000 UTC 16 Jul 1982.

b. Matching procedure

The first step is to match the radar data time with the model time. Once this is established, the model cycles through all of the grid points and the CPS is used to determine if there is convection at any given point. The flow chart in Fig. 2 shows the decision making process that follows. The easiest situation to address is that in which no radar data exist for a grid point. In that case, it is left up to the CPS to calculate, based upon the model environment, whether or not convection occurs. Beyond this, the radar data determine where convection will be.

Two courses of action can be taken where the radar data indicate there is no convection. The first, and simplest, is when the CPS also determines that no convection exists at the grid point. The scheme is simply allowed to do as it normally would and move on to the next grid point. However, if the CPS moves to initiate convection, or if convection is already in progress, it must be suppressed or stopped. This is accomplished by setting the convective tendencies (heating, moistening, etc.) in the model governing system of equations to zero.

When the radar data show convection at a grid point and the CPS produces convection, no action is taken. But when the CPS does not produce convection, it must be forced at that grid point. In this case, a criterion to select the layer most likely to be the source air must be chosen. After that, a method to force this layer to its LFC to make a convective cloud must be devised. If, after forcing the layer to its LFC, the CPS does not produce a cloud at least 4 km deep, a technique to modify the layer in order to increase its potential buoyant energy (PBE) must be formulated.

The selection of the layer to serve as the source for the convection deserves careful consideration. Two different criteria can be used to make this determination:

- 1) the layer with the highest equivalent potential temperature, or
- 2) the layer with the least amount of convective inhibition to overcome before reaching its LFC.

Both criteria were tested in a simulation of the 10–11 June 1985 squall line and were found to yield virtually identical results (Lambert 1994). Therefore, only the criterion specifying the layer with the highest equivalent potential temperature will be considered here. Typically, it is this layer that is associated with the maximum amount of PBE and is most likely the layer that produces a deep convective cloud.

c. Forcing a deep convective cloud

The first assumption made when the CPS does not produce convection where it is observed is that the estimated subgrid-scale perturbation added to the parcel, the technique used to trigger convection in the conventional KF scheme, is not large enough for the parcel to reach its LFC. Therefore, the parcel vertical velocity is arbitrarily increased to a value sufficiently large to let the parcel reach its LFC, at which time it becomes positively buoyant and can produce a convective cloud. If the cloud is at least 4 km deep, no further forcing is needed.

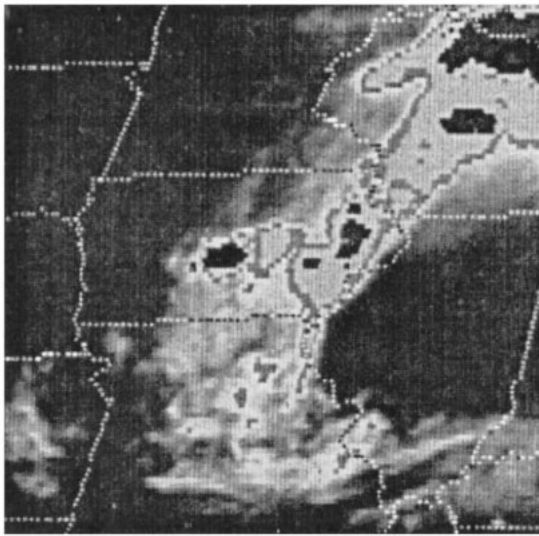
If, however, the depth of the cloud produced by the CPS is less than 4 km, or if there is no LFC, another assumption is made, that is, that the simulated moisture in the source layer is less than the moisture that was actually present. It is well known that water vapor has significant small-scale temporal and spatial variations (Lilly and Perkey 1976). It is, then, a reasonable possibility that the moisture distribution may not be represented accurately by the model grid. Therefore, moisture is added to the layer in 0.1 g kg^{-1} increments, up to a maximum of 1 g kg^{-1} , until a convective cloud at least 4 km deep is produced. If, after the addition of 1 g kg^{-1} of moisture, a sufficiently deep cloud is still not produced, the forcing is stopped and no parameterized convective effects are introduced into the resolvable scale governing system of equations.

4. Example of application of technique

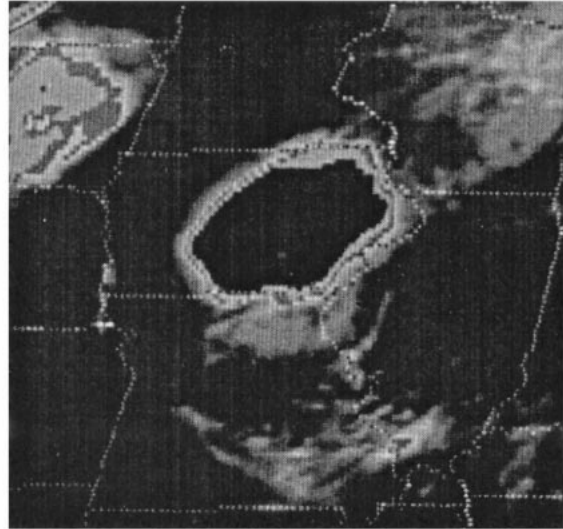
The technique described above is tested in a simulation of deep convection that occurred over the central United States during the 24-h period ending at 1200 UTC 16 July 1982. Three experiments are conducted: a control run in which no radar data were assimilated, and two experiments where radar data were assimilated for different periods of time. A description of the case and the results of the experiments follow.

a. Observational overview

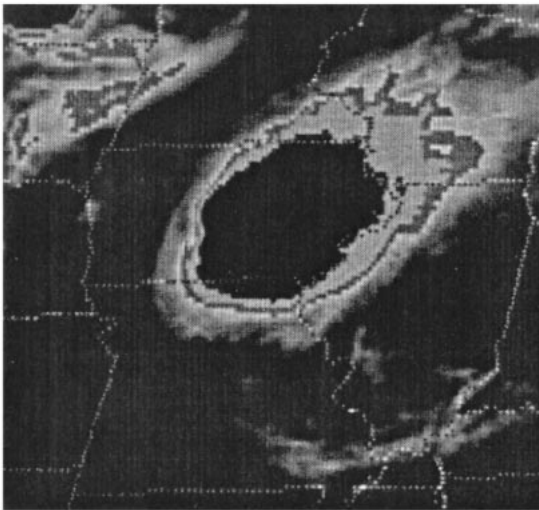
The synoptic environment at 0000 UTC 16 July, midway through the period of interest, was dominated by a large upper-level disturbance centered over south-



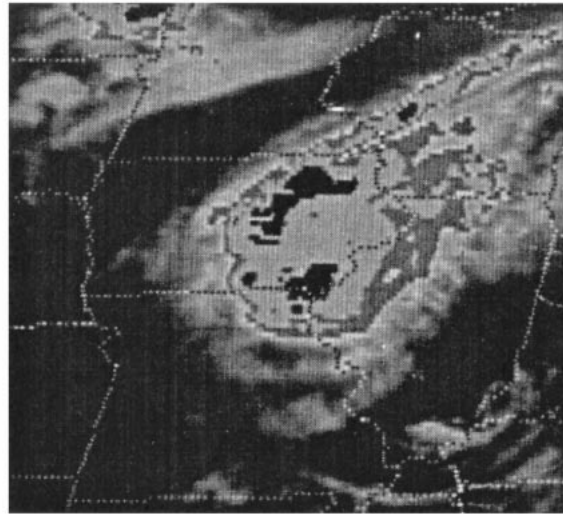
(a)



(b)



(c)



(d)

FIG. 6. Enhanced infrared satellite imagery valid at (a) 0231, (b) 0600, (c) 0900, and (d) 1201 UTC 16 Jul 1982.

western Canada and a broad surface-based high pressure system anchored over the southeastern United States. Between these two systems, the upper-level flow was primarily southwesterly with several weak mesoscale disturbances propagating out of the Rocky Mountain region and over the Great Plains. At low levels, a southerly circulation around the western side of the high pres-

sure system was advecting warm, moist air from over the Gulf of Mexico northward over the plains (Figs. 3a,b). Several mesoscale convective systems (MCSs) formed within this environment and moved eastward into the Mississippi Valley. Of particular interest is a system that developed over eastern Nebraska, north-eastern Kansas, and southwestern Iowa during the af-

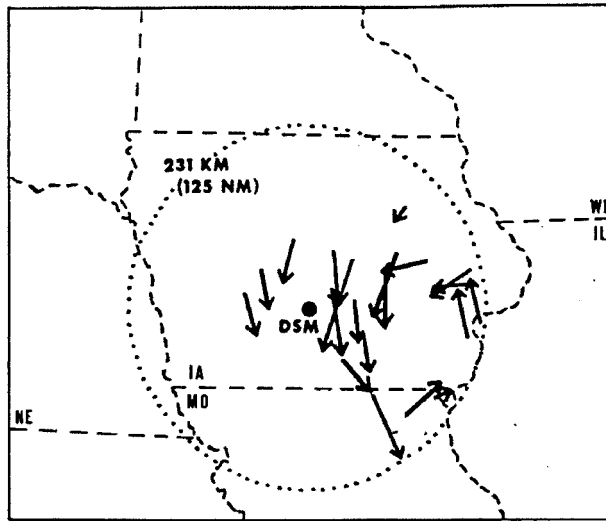


FIG. 7. Composite of Des Moines, IA, radar echo movements for 1100–1200 UTC 16 Jul 1982. Length of arrows indicates 1-h echo movement (from Fritsch et al. 1994).

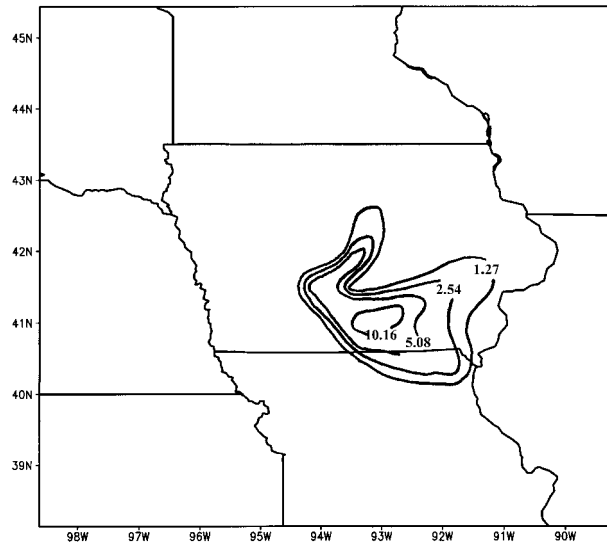


FIG. 8. Total rainfall (cm) for the 10-h period ending 1200 UTC 16 Jul 1982.

ternoon of 15 July (Fig. 4a). This system moved eastward with its leading edge reaching eastern Iowa around 0000 UTC 16 July (Figs. 4b–d). A rainfall plot for the 10-h time period corresponding to this convective system (i.e., 1400 UTC 15 July–0000 UTC 16 July; Fig. 5) shows a broad region of light rainfall covering extreme northeastern Kansas, southeastern Nebraska, northern Missouri, and much of eastern Iowa, with isolated regions of heavier rainfall in northwestern Missouri and northeastern Iowa. Evidence of this system appeared in the 0000 UTC 16 July surface analysis (Fig. 3a) as a mesohigh and an associated mesoscale cold pool. A few hours later, convection redeveloped in central Iowa and expanded into a mesoscale convective complex (MCC; Maddox 1980) with peak intensity occurring around 0900 UTC (Figs. 6a–c). By 1200 UTC, the MCC was dissipating (Fig. 6d) and a mesovortex emerged from the remnants of the system shortly thereafter (Fig. 7). A plot of precipitation for the time period corresponding to the overnight MCC (i.e., 0200 UTC–1200 UTC 16 July; Fig. 8) shows heavy rainfall in south-central Iowa, with some locations receiving more than 10 cm of rain during this 10-h time period.

b. Experimental design

Figure 9 presents the design of the experiments. For the control run (expt CTL), no radar data are used to specify convective locations (i.e., the KF parameterization scheme is free to develop convection on its own). For the two experimental runs, assimilation times of 12 and 24 h (expts RA12 and RA24, respectively) are used. For both of these experiments, the only information assimilated during the dynamic initialization period is the radar-dictated timing and location of convection.

c. Results

A plot of 10-h total (convective plus resolvable scale) rainfall ending at 0000 UTC 16 July for the three experiments is shown in Fig. 10. The most striking feature common to both experiments CTL and RA12 is the widespread area of spurious light rainfall (cf. Figs. 5 and 10) covering much of the map. Evidently, assimilating radar data for 12 h was insufficient to modify the mesoscale environment to produce an accurate forecast of rainfall. In contrast, rainfall patterns for the experiment during which radar data assimilation was still occurring (expt RA24; Fig. 10c) exhibit a much better agreement with the observed distribution of rainfall, with only a small area of spurious rainfall in northeastern Nebraska and northwestern Iowa.

The simulated sea level pressure, surface temperature, and hourly convective rainfall distributions for 0000 UTC 16 July reflect these differences among the experiments. For example, in the control run (Fig. 11)

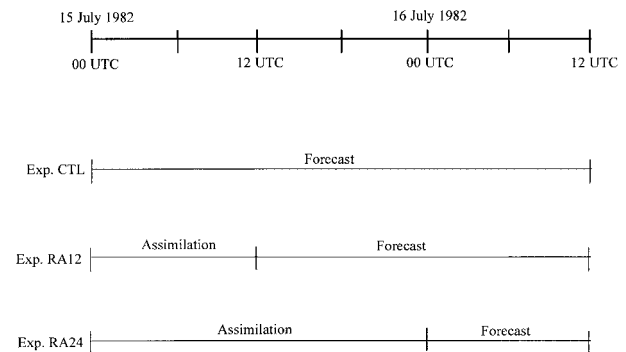


FIG. 9. Schematic representation of control (CTL) and radar assimilation (RA) experiments.

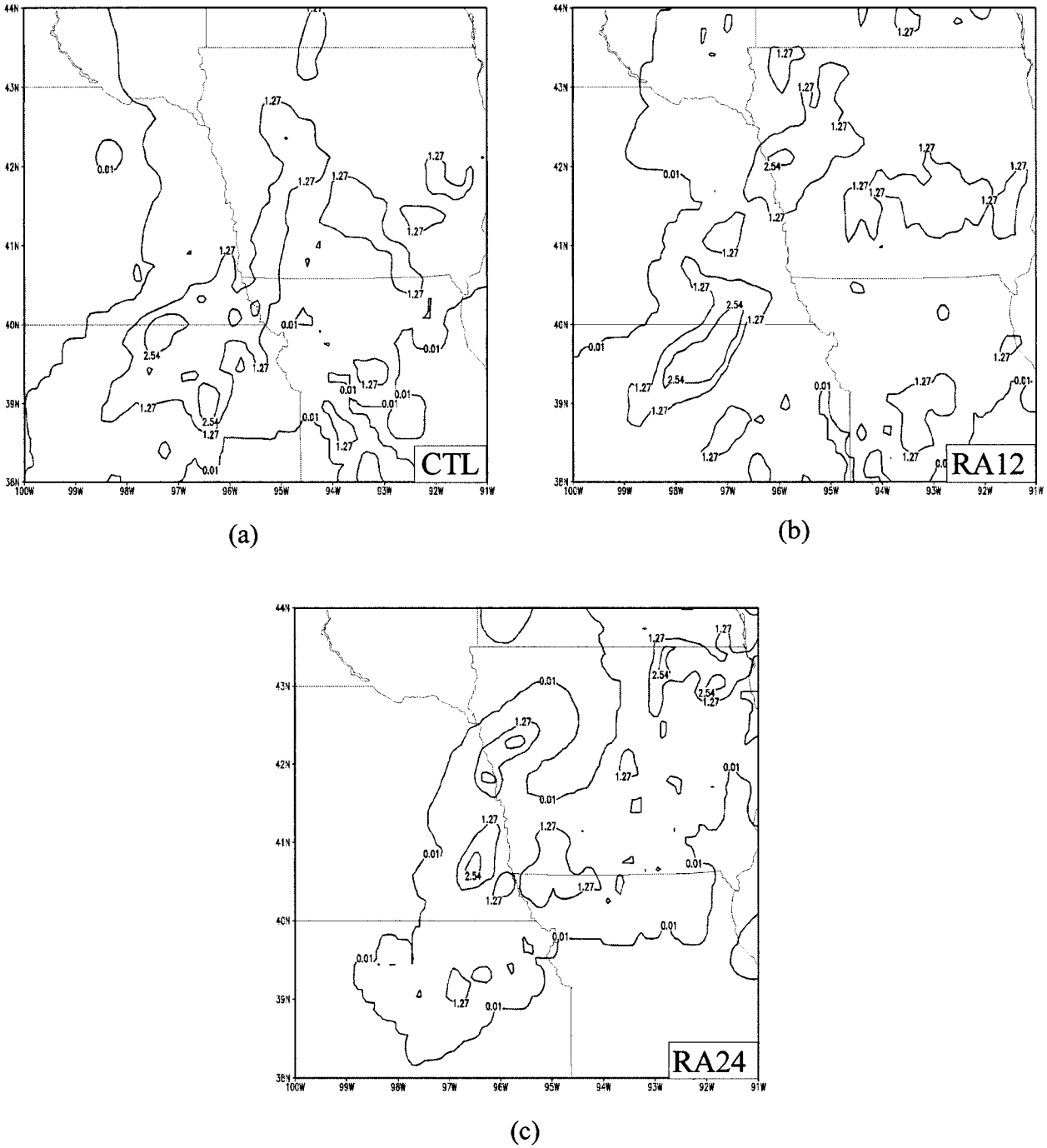


FIG. 10. Simulated total (parameterized plus resolvable scale) rainfall (cm) for the 10-h period ending at 0000 UTC 16 Jul: (a) expt CTL, (b) expt RA12, and (c) expt RA24.

much of the convective rainfall is concentrated in a line stretching from western Iowa southwestward into northeastern Kansas. Cold pools and locally higher pressures accompany the convective rainfall. Low temperatures also cover northeastern Iowa, southeastern Minnesota, and southwestern Wisconsin where clouds were blocking incoming shortwave radiation and evaporation of

resolvable-scale precipitation was occurring. When radar forcing is applied for the first 12 h of the simulation (expt RA12), less convective rainfall and a correspondingly weaker cold pool develops over western Iowa (Fig. 12); however, the broad area of cooling from radiative effects and resolvable-scale rainfall persists in southern Minnesota, southwestern Wisconsin, and northeastern

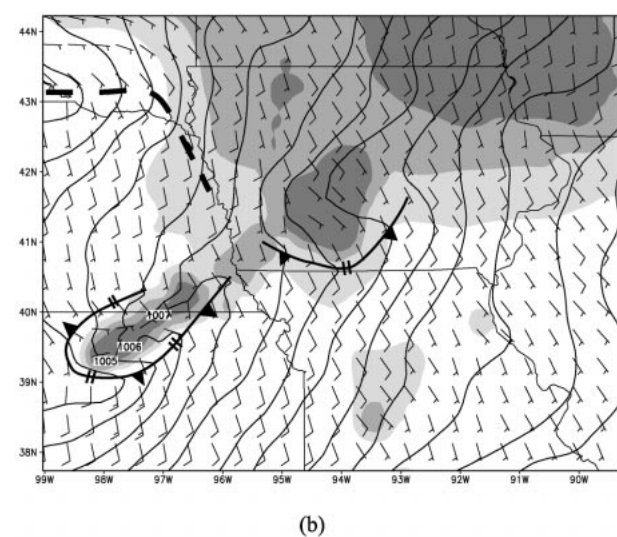
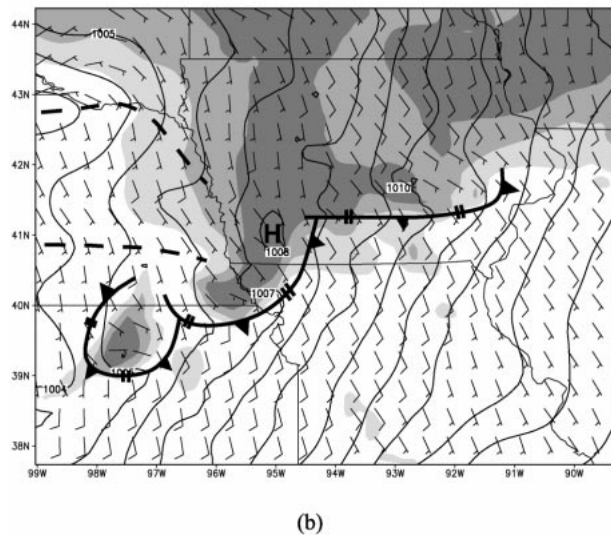
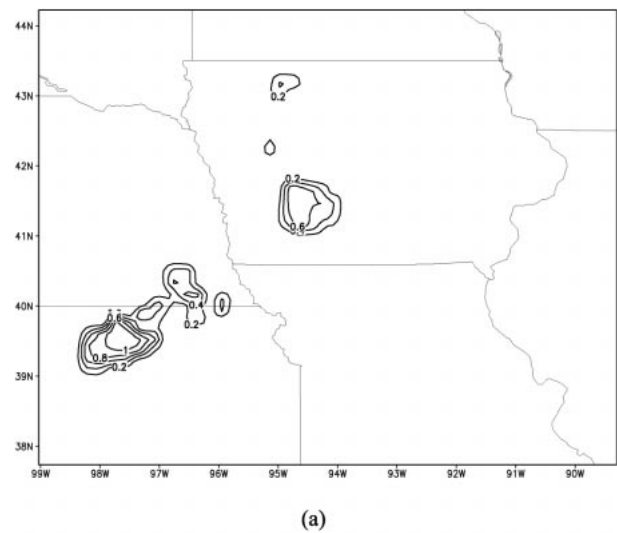
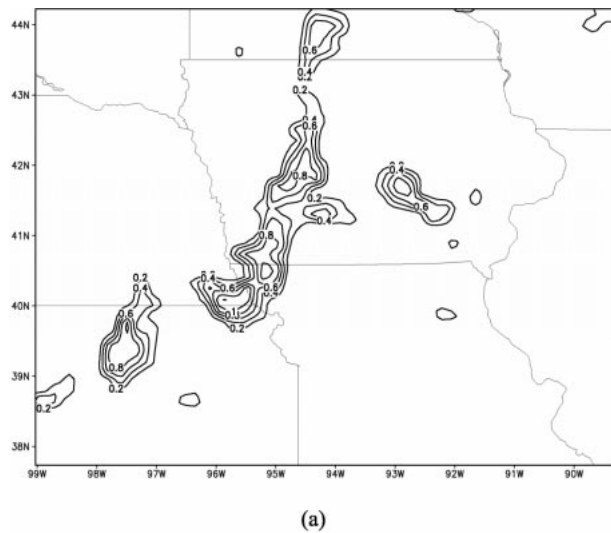


FIG. 11. (a) Simulated 1-h accumulated convective rainfall for expt CTL at 0000 UTC 16 Jul (contour interval 0.2 cm), (b) sea-level pressure (contour interval, 1 mb), winds (full barb = 5 m s⁻¹), and temperature (shading) at $\sigma = 0.997$ level. Light, medium, and dark shading denotes areas where temperatures are less than 28°, 26°, and 24°C, respectively.

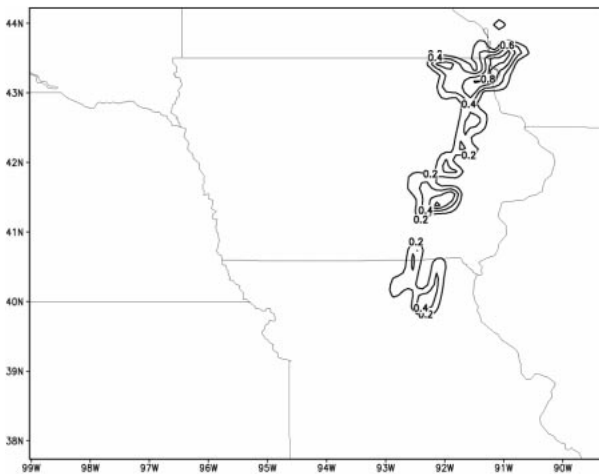
FIG. 12. Same as Fig. 8 but for expt RA12.

Iowa. When 24 h of radar forcing is applied (expt RA24), the convective rainfall shifts into eastern Iowa (Fig. 13). Since the time of the RA24 analysis is at the ending time of the radar forcing, the distribution of convective rainfall corresponds closely to the observations. Likewise, the simulated sea level pressure field and the surface-based cold pool in RA24 also resemble the observed fields (cf. Figs. 3a and 13b).

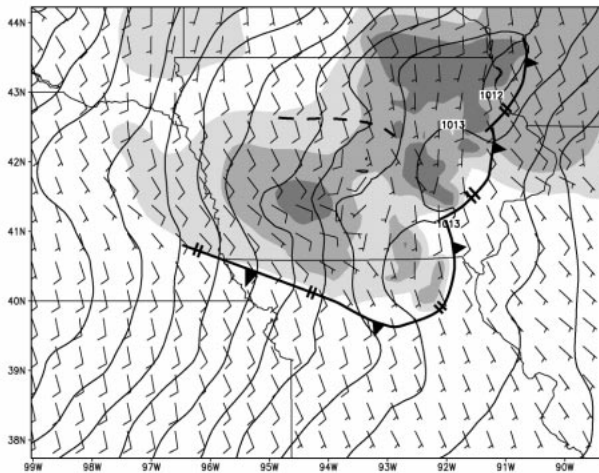
A comparison of simulated to observed total rainfall during the ensuing MCC cycle (cf. Figs. 8 and 14) shows that for all three experiments, the location of the bulk of the simulated precipitation is displaced to the northwest of the observed rainfall. This is due to the fact

that, in all of the experiments, the placement of the low-level jet is to the west of its observed location (not shown). Despite this systematic error, improvements in the rainfall distribution do occur when radar assimilation is used. Specifically, the precipitation pattern changes from an elongated swath of rainfall that stretches across parts of several states (expt CTL) to a more compact pattern where the heavy rainfall is concentrated primarily in Iowa (expt RA24). Qualitatively, the pattern from experiment RA24 is in better agreement with the observations, even producing the 10-cm maximum that was observed.

In addition to the changes in rainfall, sea level pressure, and surface temperature, the radar data assimilation also forces changes in the winds aloft. For example, Fig. 15 shows the 1200 UTC 16 July winds and relative vorticity at the $\sigma = 0.5$ level (approximately 500 mb)



(a)



(b)

FIG. 13. Same as Fig. 8 but for expt RA24.

for the three simulations. The most obvious difference is that, without the radar information, the model fails to create the midlevel mesovortex observed in the satellite and radar data [see Fig. 7 and Fritsch et al. (1994)]. When radar information is assimilated for 24 h, the model produces a midlevel cyclonic circulation with a diameter of approximately 200 km, closely agreeing with the size of the observed vortex as inferred by the motion of the radar echoes (Fig. 7), albeit displaced to the northwest. The development of this mesovortex is especially critical since, as shown in Fritsch et al. (1994), the vortex persisted for 36 more hours and was instrumental in organizing multiple outbreaks of deep convection, one of which produced over 25 cm of rain and flash floods in southern Michigan.

5. Summary and discussion

A procedure that uses radar reflectivity observations to help initialize a mesoscale model during a preforecast period was documented. Unlike previous studies, the radar data are not used to infer rain rates and heating profiles. Rather, the data are only used to tell the model when and where deep moist convection is occurring in a preforecast period. The model's convective parameterization scheme is then manipulated to turn on or off in a manner that matches the timing and location of the observed convection. The performance of the technique was demonstrated in a set of numerical experiments on a case involving organized deep convection in a warm-season environment. The results indicate that radar data, when used to regulate when and where the model's convective parameterization is applied, can be instrumental in improving forecasts of mesoscale weather features. Simulations of sea level pressure, surface temperature, rainfall, and midlevel winds all were improved when radar data were assimilated for 24 h.

The displacement of the rainfall and midlevel cyclonic circulation during the MCC cycle, common to all three simulations, highlights an important limitation to this technique; that is, the effectiveness of assimilating radar data is diminished in situations where the environment is strongly forced but captured poorly by the model. In such a situation, it is difficult to force parameterized convection to follow a solution that agrees with the observed distribution of convection. When this occurs, it is possible that severe imbalances would be created in areas where the model dynamics and thermodynamics do not support the decisions being specified by the radar assimilation scheme. The result is a convectively modified environment that does not agree with the (incorrect) mesoscale environment of the simulation. For the example shown here, one of the major environmental features responsible for organizing the convection was the low-level jet. Since none of the simulations captured the exact location of the jet at 0000 UTC 16 July, none of the simulations produced rainfall in the proper location after this time.

Conversely, the effectiveness of the technique is enhanced in weakly forced environments where convective initiation and organization are governed by previous convective activity. This aspect of convective forecasting was alluded to in Stensrud and Fritsch (1994a), who showed that great difficulties sometimes arise from the lack of observations of ongoing mesoscale forcing during the period of model initialization. Because these circulations are often dependent upon convectively induced mesoscale features (such as mesohighs and outflow boundaries) that typically are not included in the initial conditions, there is little prospect that the requisite mesoscale circulations will ever develop at the appropriate location and in a timely manner. Application of the technique presented here would improve the specification of these features, resulting in an improved sim-

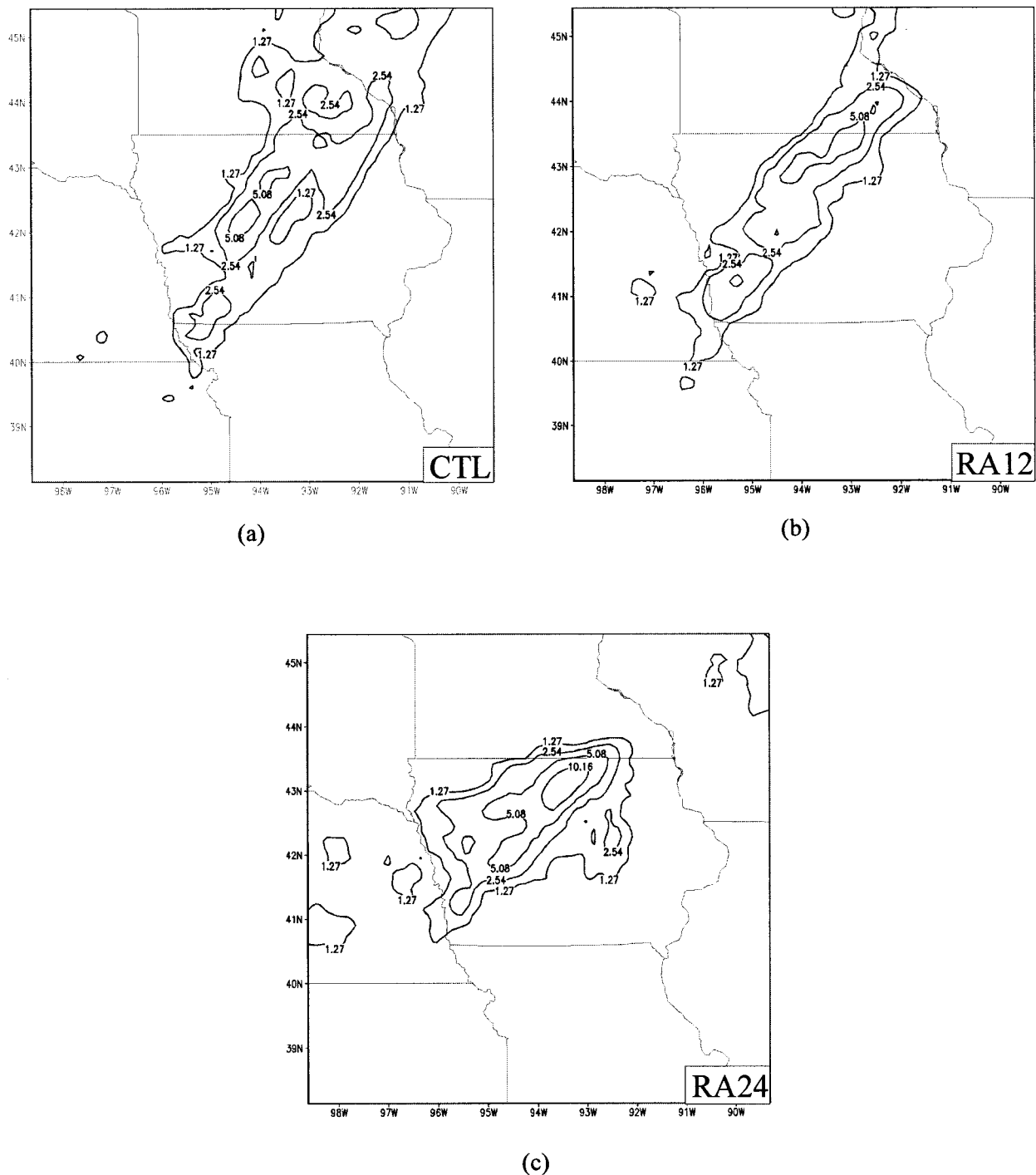


FIG. 14. Same as Fig. 9 but for the 10-h period ending at 1200 UTC 16 Jul: (a) expt CTL, (b) expt RA12, and (c) expt RA24.

ulation of subsequent convective activity. In the example shown here, the correct location and strength of the mesohigh and surface-based cold pool at 0000 UTC 16 July in experiment RA24 was responsible for producing a pattern and intensity of rainfall that was much closer to the observations, even if its location was displaced from the observed location due to the displace-

ment of the low-level jet. In contrast to the improvements in the rainfall pattern and amounts prior to 1200 UTC 16 July that accompanied experiment RA24, relatively little improvement occurred in the rainfall fields for the 10-h time period prior to 0000 UTC 16 July for experiment RA12. This lack of improvement could be due to several factors such as, for example, the amount

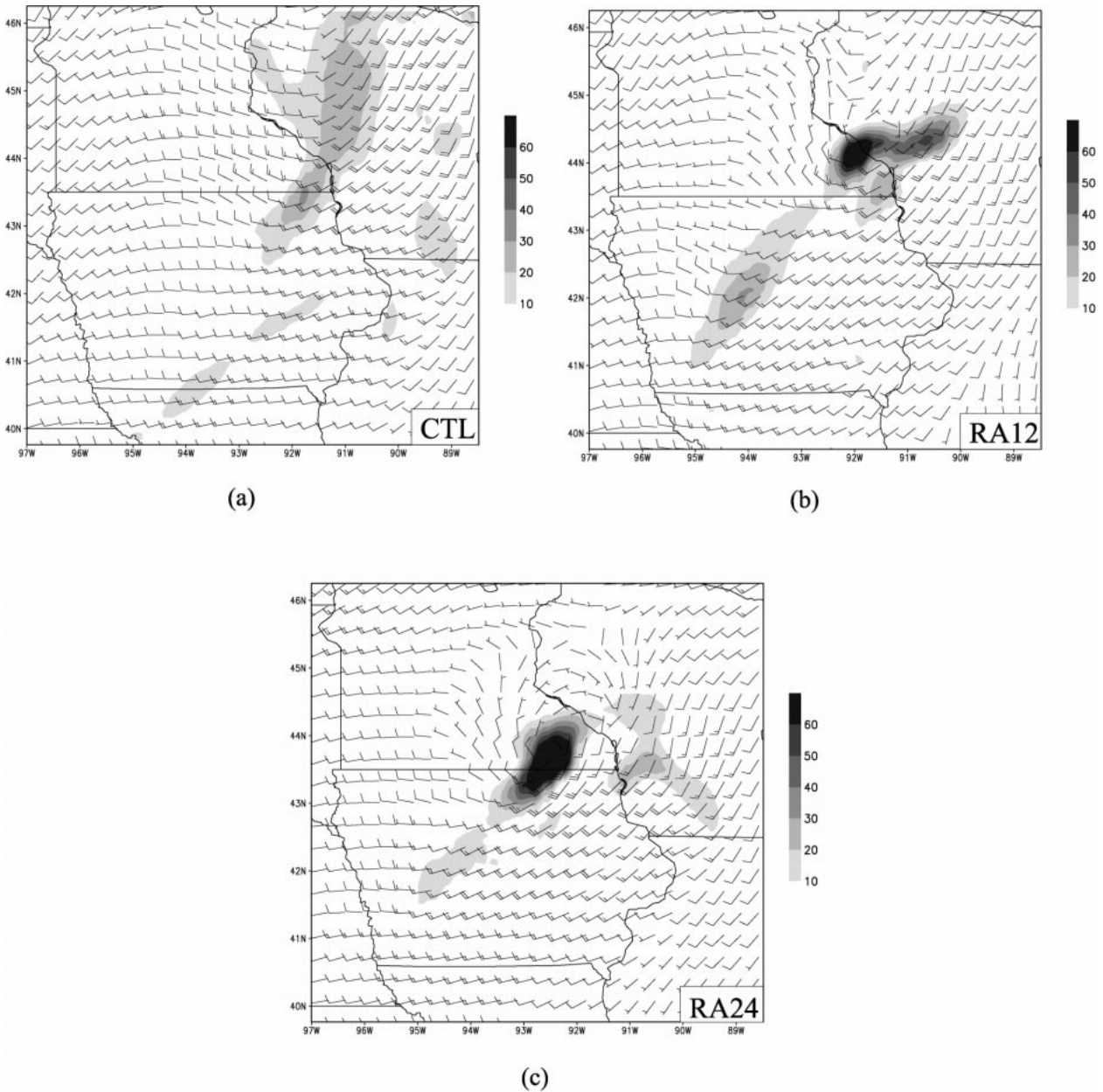


FIG. 15. Simulated wind fields (full barb = 10 m s^{-1}) and relative vorticity (shading, $\times 10^{-5} \text{ s}^{-1}$) at the $\sigma = 0.5$ level (about 500 mb) for 1200 UTC 16 Jul: (a) expt CTL, (b) expt RA12, and (c) expt RA24.

of time required for the mass-field changes imposed by the convective parameterization to affect the wind field and achieve a new (convectively modified) balanced state. Alternatively, it may simply be due to the fact that the importance of the convectively induced features in governing subsequent convective activity is less at 1200 UTC 15 July than it is at 0000 UTC 16 July, if only because surface-based cold pools and outflow boundaries are weaker during the overnight hours than they are during the late afternoon.

The major advantage of this technique is its simplicity. Heating rates based on rain rates that are, in turn,

based on radar reflectivity do not have to be derived and added to the thermodynamic equation. Furthermore, vertical heating profiles, which can vary considerably from case to case (Kain and Fritsch 1990), do not have to be specified. Moreover, the technique can be easily automated and introduced as part of a model data assimilation system. In an operational mode, radar data could be continuously assimilated into a forecast model so that, at any given initialization time, the convective environment would reflect the accumulated effects of convection on the local environment for an extended period of time. Finally, the technique could easily be

adapted to other convective parameterization schemes, provided the trigger function for the scheme provides a method for forcing parameterized convection. Of course, schemes that do little to modify the local environment when convection occurs (such as schemes without parameterized downdrafts) would see their effectiveness reduced when radar assimilation is employed.

A disadvantage of the proposed technique is that, other than identifying the location of active convection, the magnitude of the reflectivity values is not utilized. Thus, the intensity of the convection is highly dependent on the accuracy of the model's forecast of the mesoscale environment and on the accuracy of the CPS. One possible way to address this problem would be to increase the low-level moisture (and hence the low-level θ_e) by a factor that is a function of the intensity of the radar echoes. This should be a topic for further study. Another potential area for improvement involves the adjustment to the moisture values of the source-layer air when the radar data indicate convection is occurring at a grid point but it is not supported by the parameterization scheme. Rather than only modifying the specific grid point, the effects of this moistening could be spread over a larger horizontal area. Finally, there may be areas in the model grid in which there is no radar data. However, this would be a problem for all radar data assimilation techniques. A more general solution would be to extend the technique so that it can be used with satellite data, especially over data-sparse regions.

It is recognized, of course, that examination of this technique in a single case prevents a comprehensive assessment of the effectiveness and robustness of the technique. Multiple cases, spanning a variety of convective environments, must be simulated in order to make an adequate assessment of the efficacy of the technique. While the case shown here provided valuable insight into situations in which the technique would be most (and least) helpful, further testing is certainly required.

Acknowledgments. This work was supported by NSF Grant ATM 92-22017 and NASA Grant NAG 5-2927.

REFERENCES

- Anthes, R. A., 1977: A cumulus parameterization scheme utilizing a one-dimensional cloud model. *Mon. Wea. Rev.*, **105**, 270–286.
- Aonashi, K., 1993: An initialization method to incorporate precipitation data into a mesoscale numerical weather prediction model. *J. Meteor. Soc. Japan*, **71**, 393–406.
- Charney, J. G., M. Halem, and R. Jastrow, 1969: Use of incomplete historical data to infer the present state of the atmosphere. *J. Atmos. Sci.*, **26**, 1160–1163.
- Dudhia, J., 1989: Numerical study of convection observed during the Winter Monsoon Experiment using a mesoscale two-dimensional model. *J. Atmos. Sci.*, **46**, 3077–3107.
- , and —, 1981: Preliminary numerical tests of the modification of mesoscale convective systems. *J. Appl. Meteor.*, **20**, 910–921.
- , J. D. Murphy, and J. S. Kain, 1994: Warm core vortex amplification over land. *J. Atmos. Sci.*, **51**, 1780–1807.
- Grell, G. A., J. Dudhia, and D. R. Stauffer, 1994: A description of the fifth-generation Penn State/NCAR Mesoscale Model (MM5). NCAR Tech. Note NCAR/TN-398+1A, 117 pp.
- Jastrow, R., and M. Halem, 1970: Simulation studies related to GARP. *Bull. Amer. Meteor. Soc.*, **51**, 490–513.
- Kain, J. S., and J. M. Fritsch, 1990: A one-dimensional entraining/detraining plume model and its application in convective parameterization. *J. Atmos. Sci.*, **47**, 2784–2802.
- , and —, 1992: The role of the convective “trigger function” in numerical forecasts of mesoscale convective systems. *Meteor. Atmos. Phys.*, **49**, 93–106.
- Kasahara, A., A. P. Mizzi, and L. J. Donner, 1994: Diabatic initialization for improvement in the tropical analysis of divergence and moisture using satellite radiometric imagery data. *Tellus*, **46A**, 242–264.
- Koch, S. E., A. Ahmet, and J. T. McQueen, 1997: The influence of mesoscale humidity and evapotranspiration fields on a model forecast of a cold-frontal squall line. *Mon. Wea. Rev.*, **125**, 384–409.
- Krishnamurti, T. N., J.-S. Xue, H. S. Bedi, K. Ingles, and D. Oosterhof, 1991: Physical initialization for numerical weather prediction over the tropics. *Tellus*, **43AB**, 53–81.
- Lambert, W. C., 1994: A procedure for using radar reflectivity data to locate convection in the dynamic initialization of a mesoscale model. M.S. thesis, Dept. of Meteorology, The Pennsylvania State University, University Park, 110 pp. [Available from The Pennsylvania State University, Dept. of Meteorology, University Park, PA 16802.]
- Lewis, J. M., and J. C. Derber, 1985: The use of adjoint equations to solve a variational adjustment problem with advective constraints. *Tellus*, **37A**, 309–322.
- Lilly, D., and D. Perkey, 1976: Sensitivity of mesoscale predictions to mesoscale initial data. Preprints, *Sixth Conf. on Weather Forecasting and Analysis*, Albany, NY, Amer. Meteor. Soc., 174–179.
- Lyne, W. H., R. Swinbank, and N. T. Birch, 1982: A data assimilation experiment and the global circulation during the FGGE special observing periods. *Quart. J. Roy. Meteor. Soc.*, **108**, 575–594.
- Maddox, R. A., 1980: Mesoscale convective complexes. *Bull. Amer. Meteor. Soc.*, **61**, 1374–1387.
- Manobianco, J., S. Koch, V. M. Karyampudi, and A. J. Negri, 1994: The impact of assimilating satellite-derived precipitation rates on numerical simulations of the ERICA IOP 4 cyclone. *Mon. Wea. Rev.*, **122**, 341–365.
- Meitin, J. G., and J. B. Cuning, 1985: The Oklahoma–Kansas preliminary regional experiment for STORM-CENTRAL (O-K PRE-STORM). Vol. I. Daily operations summary. NOAA Tech. Memo. ERL ESG-20, Boulder, CO, 313 pp.
- Puri, K., and N. E. Davidson, 1992: The use of infrared satellite cloud imagery data as proxy data for moisture and diabatic heating in data assimilation. *Mon. Wea. Rev.*, **120**, 2329–2341.
- Rogers, R. F., 1998: Amplification of warm-core vortices by convective redevelopment: A key component of tropical cyclogenesis. Ph.D. thesis, The Pennsylvania State University, University Park, PA, 196 pp. [Available from The Pennsylvania State University, University Park, PA 16802.]
- , and J. M. Fritsch, 1996: A general framework for convective trigger functions. *Mon. Wea. Rev.*, **124**, 2438–2452.
- Rutledge, S. A., and D. B. MacGorman, 1988: Cloud-to-ground lightning activity in the 10–11 June 1985 mesoscale convective system observed during the Oklahoma–Kansas PRE-STORM project. *Mon. Wea. Rev.*, **116**, 1393–1408.
- Stauffer, D. R., and N. L. Seaman, 1990: Use of four-dimensional data assimilation in a limited-area mesoscale model. Part I: Experiments with synoptic-scale data. *Mon. Wea. Rev.*, **118**, 1250–1277.
- Stensrud, D. J., and J. M. Fritsch, 1994a: Mesoscale convective systems in weakly forced large-scale environments. Part II: Gen-

- eration of mesoscale initial conditions. *Mon. Wea. Rev.*, **122**, 2068–2083.
- , and —, 1994b: Mesoscale convective systems in weakly forced large-scale environments. Part III: Numerical simulations and implications for operational forecasting. *Mon. Wea. Rev.*, **122**, 2084–2104.
- Takano, I., and A. Segami, 1993: Assimilation and initialization of a mesoscale model for improved spin-up of precipitation. *J. Meteor. Soc. Japan*, **71**, 377–391.
- Wang, W., and T. T. Warner, 1988: Use of four-dimensional data assimilation by Newtonian relaxation and latent-heat forcing to improve a mesoscale-model precipitation forecast: A case study. *Mon. Wea. Rev.*, **116**, 2593–2613.
- Zhang, D.-L., 1989: The effect of parameterized ice microphysics on the simulation of vortex circulation with a mesoscale hydrostatic model. *Tellus*, **41A**, 132–147.
- , and R. A. Anthes, 1982: A high resolution model of the planetary boundary layer—Sensitivity tests and comparisons with SESAME-79 data. *J. Appl. Meteor.*, **21**, 1594–1609.
- , and J. M. Fritsch, 1986: Numerical simulation of the meso- β scale structure and evolution of the 1977 Johnstown flood. Part I: Model description and verification. *J. Atmos. Sci.*, **43**, 1913–1943.
- , and R. Harvey, 1995: Enhancement of extratropical cyclogenesis by a mesoscale convective system. *J. Atmos. Sci.*, **52**, 1107–1127.
- , H.-R. Chang, N. L. Seaman, T. T. Warner, and J. M. Fritsch, 1986: A two-way interactive nesting procedure with variable terrain resolution. *Mon. Wea. Rev.*, **114**, 1330–1339.